NANOSYSTEMS:
PHYSICS, CHEMISTRY, MATHEMATICS

Mamanazirov J., et al. *Nanosystems: Phys. Chem. Math.*, 2025, **16** (6), 887–896.
http://nanojournal.ifmo.ru
DOI 10.17586/2220-8054-2025-16-6-887-896

Original article

MXene based electrocatalysts for efficient water splitting

Javlonbek Mamanazirov[1,2,a], Shavkat Mamatkulov[1,7,b], Maxfuza Jumayeva[1,c], Khakimjan Butanov[1,d], Wen He[3,e], Jingxiang Low[4,f], Odilhuja Parpiev[1,g], Olim Ruzimuradov[6,h]

[1]Institute of Materials Science, Uzbekistan Academy of Sciences, Tashkent, Uzbekistan

[2]National Research Institute of Renewable Energy Sources, Ministry of Energy, Tashkent, Uzbekistan

[3]School of Materials Science and Engineering, Anhui University, Hefei, China

[4]School of Physical Science and Technology, Tiangong University, Tianjin, China

[5]Alfraganus University, Tashkent, Uzbekistan

[6]Turin Polytechnic University in Tashkent, Tashkent, Uzbekistan

[7]Institute of Fundamental and Applied Research under TIIAME National Research University, Tashkent, Uzbekistan

[a]j.mamanazirov@imssolar.uz, [b]mi-shavkat@yandex.ru, [c]m.jumayeva1988@gmail.com, [d]kh.butanov@gmail.com, [e]hewen@ahu.edu.cn, [f]jxlow@ustc.edu.cn, [g]o.parpiev@imssolar.uz, [h]o.ruzimuradov@polito.uz

Corresponding author: J. Mamanazirov, j.mamanazirov@imssolar.uz

ABSTRACT In this study, we modified Ni based electrodes with MXene and MXene-based composite catalysts for water splitting. The MXene based catalyst exhibited excellent electrochemical surface area (ECSA) of 1840 cm^2, highlighting its abundant active sites. To further enhance catalytic activity, MXene was modified with graphene oxide (GO) and carbon black (CB), which significantly reduced the overpotential from 300 mV to 196 mV at 10 mA cm^{-2} and improved the reaction kinetics, as evidenced by a low Tafel slope of 96.35 mV dec^{-1}. Moreover, the MXene–GO–CB composite demonstrated outstanding long-term durability, maintaining stable operation for 50 h at 100 mA cm^{-2} with only a 34 mV increase in overpotential at 10 mA cm^{-2}. These results confirm that the synergistic combination of MXene with GO and CB yields a highly active and durable electrocatalyst, offering strong potential for practical water electrolysis applications.

KEYWORDS MXene based composites, HER, OER, electrocatalysts.

ACKNOWLEDGEMENTS The authors gratefully acknowledge the support of the Agency of Innovative Development under the Ministry of Higher Education, Science and Innovation of the Republic of Uzbekistan within the framework of research project No. ALM-20230502808. This support made the successful completion of this work possible.

FOR CITATION Javlonbek Mamanazirov, Shavkat Mamatkulov, Maxfuza Jumayeva, Khakimjan Butanov, Wen He, Jingxiang Low, Odilhuja Parpiev, Olim Ruzimuradov MXene based electrocatalysts for efficient water splitting. *Nanosystems: Phys. Chem. Math.*, 2025, **16** (6), 887–896.

1. Introduction

The transition to sustainable energy sources requires the development of efficient and environmentally friendly technologies for hydrogen production. Water electrolysis, particularly when powered by renewable energy sources, is considered one of the most promising routes for hydrogen generation [1–4]. However, the widespread implementation of this technology is hindered by the necessity of using expensive and scarce metals, such as platinum, ruthenium, iridium, etc. as catalysts for the hydrogen evolution reaction (HER) [5–7]. As a result, intensive efforts are being made to find alternative materials that combine high catalytic activity, stability in harsh environments, and cost-effectiveness. Among such materials, MXenes — two-dimensional transition metal carbides — have attracted significant attention due to their high electrical conductivity, large surface area, and tunable surface chemistry through functional group modification. In particular, $Ti_3C_2T_x$ has demonstrated promising properties as a catalyst for HER [8–19]. Nevertheless, the overtime oxidation of MXenes in aqueous environments limits their long-term stability and catalytic efficiency [20–22]. Various electrode architectures based on combinations of MXenes with other materials have been reported. For instance, in the work by Gao et al. [23] an electrode composed of MXene and carbon nanotubes exhibited high HER activity but limited stability in alkaline media. In another study by Meng et al. [24] the use of MXene combined with metal-organic frameworks resulted in good initial performance, but the material quickly degraded under prolonged operation. These findings highlight the need for more stable composite structures.

To improve the stability of MXene-based catalysts, different strategies have been explored, including the formation of composites with other functional materials [25–27]. The incorporation of graphene oxide (GO) has shown to enhance structural stability and oxidation resistance by forming a protective matrix that slows down the degradation of MXene. Its hydrophilic surface and low work function make it an ideal component for tuning the electronic properties of active sites in composite catalysts, thereby improving their catalytic efficiency. Furthermore, the addition of carbon black (CB) can enhance the catalytic performance by improving electrical conductivity, while GO stabilizes the catalyst structure by preventing nanoparticle aggregation and providing mechanical reinforcement. Its functional groups (–OH, –COOH, –C=O) facilitate strong interactions with materials such as MXene, improving dispersion and structural integrity [28–31]. GO offers corrosion resistance in harsh electrochemical environments, increases hydrophilicity, and promotes ion transport, all contributing to enhanced electrochemical performance [32–34]. In addition, the use of nickel foam as a substrate provides mechanical strength and a three-dimensional porous architecture, which supports efficient mass transport [35–38]. The synergistic combination of MXene, CB, and GO on a nickel foam (NF) substrate can significantly enhance water electrolysis efficiency.

In this work, we developed an advanced MXene based electrocatalyst incorporating carbon black (CB) and graphene oxide (GO) to address the limitations of conventional nickel foam (NF) electrodes. The synthesis involved selectively etching the MAX phase to obtain MXene, followed by its deposition onto NF along with CB and GO to enhance conductivity, catalytic activity, and stability. The resulting MXene electrode demonstrated overpotentials of 300 mV for the hydrogen evolution reaction (HER) at 10 mA/cm^2, with Tafel slopes of 113.57 mV/dec, indicating efficient charge transfer kinetics. Integration of GO and CB into the MXene composite (MXene-GO-CB) achieving significantly lower overpotentials of 196 mV for HER at the same current density and 96.35 mV/dec Tafel slope. Electrochemical impedance spectroscopy (EIS) and electrochemically active surface area (ECSA) analysis confirmed the enhanced performance, with the MXene/NF electrode exhibiting low charge transfer resistance and high surface area (ECSA) values of 1840 cm^2, ensuring efficient reaction kinetics.

2. Experimental section

2.1. Materials

All chemicals and materials used in this study were of analytical grade. Ti_3AlC_2 MAX phase was purchased from Laizhou Kai Kai Ceramic Materials Co. Ltd. (China) with a purity of $>$99 wt% and molecular weight (MW) of 194.6 g/mol. Hydrochloric acid (HCl, 37%) was obtained from Sinopharm Chemical Reagent Co., Ltd. (China) and used as an etchant for the selective removal of the A-site element from the MAX phase. Lithium fluoride (LiF, 99%), with an MW of 25.94 g/mol, was purchased from Shanghai Macklin Biochemical Technology Co., Ltd. for the synthesis of $Ti_3C_2T_x$ MXene. For the fabrication of composite electrodes, carbon black (CB) were obtained from Sigma-Aldrich. Nickel foam (NF) with a high porosity structure was used as a conductive substrate for the deposition of MXene-based materials. Deionized (DI) water was used in all synthesis and washing processes to ensure the removal of residual chemicals and maintain the purity of the synthesized MXene.

2.2. Synthesis of MXene

To synthesize $Ti_3C_2T_x$ MXene, the selectively etching method is used. Initially, 30 mL of HCl was combined with 10 mL of deionized water, followed by the addition of 2 mg LiF to the HCl solution, which was stirred for 1 hour. Subsequently, 2 g of Ti_3AlC_2 powder was gradually added into this solution and allowed to stir at room temperature for 29 hours. The resulting suspension was then washed repeatedly with deionized water, centrifuged, and sonicated multiple times to achieve exfoliation of $Ti_3C_2T_x$ into nanosheets, continuing until the pH of the supernatant reached 6–7. The final supernatant was dispersed in water to yield a solution with a concentration of 1.5 mg mL^{-1}. This MXene solution was then freeze-dried to obtain a fluffy powder form.

2.3. Synthesis of GO

In a typical procedure, 1 g of graphite powder was added to a mixture of sulfuric acid and orthophosphoric acid (9:1, 90 mL:10 mL) under continuous stirring in an ice bath maintained at 0°C for 15 minutes. The mixture was stirred with a magnetic stirrer to ensure uniform dispersion. Subsequently, 6 g of potassium permanganate ($KMnO_4$) was gradually introduced into the solution while maintaining the temperature between 0–5°C, followed by continuous stirring for 2 hours. Afterward, the reaction was stirred at room temperature for 30 minutes and then heated to 35°C by immersing the flask in warm water, with stirring continued for another 30 minutes. The oxidation process was further advanced by heating the mixture in an oil bath at 90°C, where 46 mL of deionized (DI) water was slowly added, followed by stirring for 30 minutes. To terminate the reaction, an additional 180 mL of DI water and 10 mL of 30% hydrogen peroxide (H_2O_2) were added, leading to a color change from dark brown to yellow. The reaction was allowed to cool to room temperature before purification. The obtained suspension was washed with 200 mL of 5% HCl and deionized water several times to remove residual ions and acids. Finally, the GO product was filtered and dried at 60°C for 24 hours to obtain a fine powder.

2.4. Synthesis of MXene/NF electrode

Immersing method is used to prepare MXene/NF electrode for experiments [39]. Initially, the nickel foam (NF) was immersed in 3 M HCl solution for 2 hours to remove impurities and oxides. This was followed by ultrasonic cleaning in acetone, ethanol, and deionized water for 15 minutes each, then drying at 60°C in an oven. The cleaned NF was subsequently immersed in a $Ti_3C_2T_x$ MXene solution (4 mg mL^{-1}) for 1 hour, followed by vacuum drying for 12 hours, yielding the MXene/NF electrode.

2.5. Synthesis of MXene-GO-CB/NF and other composite electrodes

A stock solution of synthesized MXene (1.6 mg mL^{-1}) was prepared, while graphene oxide (GO, 4 mg mL^{-1}) and carbon black (CB, 4 mg mL^{-1}) were dispersed separately in 10 mL deionized water. To fabricate the MXene–GO–CB composite electrode, 25 mL of the MXene solution was mixed with 0.25 mL of GO and 0.25 mL of CB solutions, followed by ultrasonication for 10 min to ensure homogeneous dispersion. Nickel foam (NF) substrates were immersed in the resulting suspension for 1 h and then dried in an oven under continuous argon flow, where the temperature was gradually increased to 170°C and maintained for 24 h. For comparison, MXene–CB and MXene–GO electrodes were prepared using the same procedure but without the addition of GO and CB, respectively.

2.6. Electrochemical analysis

Electrochemical measurements were carried out on a CHI760E electrochemical workstation (China) in 1 M KOH electrolyte under iR-corrected conditions. A three-electrode configuration was employed, in which the synthesized MXene based electrodes served as the working electrodes (WE), a platinum foil was used as the counter electrode (CE), and an Ag/AgCl electrode functioned as the reference electrode (RE). The measured potentials (E_m) were converted to the reversible hydrogen electrode (RHE) scale according to the equation: E vs RHE = E_{SHE} + $E_{Ag/AgCl}$+ 0.059 x pH and pH = 14 for 1 M KOH. The mass loading of the active material on the NF substrate was 0.015 mg cm^{-2} for the MXene–GO–CB/NF electrode. Geometric area of the prepared electrodes are 1.6 cm^2. In order to approximate the empirical data of EIS, Randles electrical circuit was used.

3. Results and discussion

SEM image (Fig. 1) shows a well-formed MAX phase material, displaying the characteristic layered morphology of alternating (M) and (A) element layers, typical of Ti_3AlC_2. The undulating texture with intact stratifications indicates a stable structure, with no signs of delamination, which aligns with the material being a MAX phase rather than an etched MXene. The small particles observed on the surface could be residual synthesis by-products or minor impurities. At 10,000x magnification, the continuity and integrity of the layers suggest good sample quality, with well-preserved lamellar features that support the robustness of MAX phase properties. Fig. 1b shows the morphology of exfoliated $Ti_3C_2T_x$ MXene synthesized by selective etching of MAX with HCl and LiF. The images reveal well-defined, with large surface area, and thin single-layer MXene sheets with a lateral size in the 10 μm range.

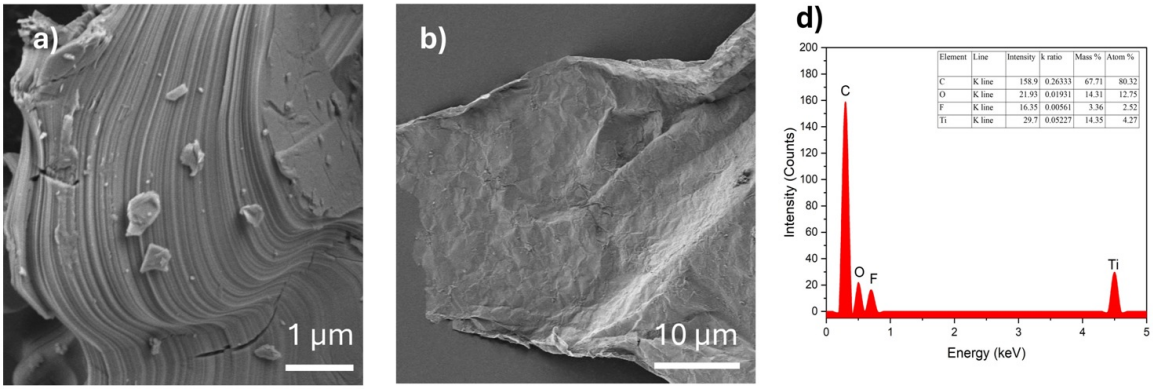

FIG. 1. (a) SEM image of the MAX phase, showing a layered structure. (b) Single-layer MXene sheets. (d) EDX spectrum of MXene, confirming the presence of Ti, C, O, F

The clear exfoliation and separation of individual layers are characteristic of successful delamination, where the thickness of each layer is approximately 1–2 nm, consistent with literature reports for monolayer $Ti_3C_2T_x$ [40]. The wrinkled and crumpled nature of the flakes suggests flexibility and structural integrity at the nanoscale, which are common features of MXene sheets [41]. These characteristics, coupled with the absence of aggregation, confirm the successful synthesis of high-quality, monolayer MXene, a key factor in maximizing surface area and ensuring optimal electrochemical performance in potential applications [42]. The EDS analysis in Fig. 1d and elemental mapping presented in Fig. 2 show that the elements of the material are evenly distributed and the $Ti_3C_2T_x$ MXene was functionalized [43]. By using HCl and LiF,

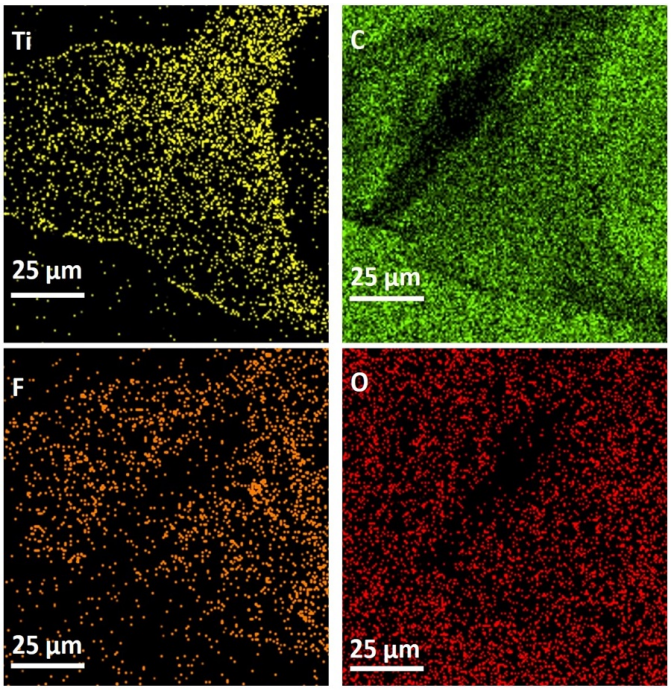

FIG. 2. EDS elemental mapping of $Ti_3C_2T_x$ MXene, showing the distribution of different elements

the aluminium layers were effectively removed from the MAX phase [44]. The high carbon content (80.32 at%) and its predominant presence in the mapping, represented in green, confirm the retention of the carbon layers, essential for the 2D structure and electrical conductivity of MXene [45]. Titanium (4.27 at%) is evenly distributed, as shown in yellow, supporting the structural integrity of the Ti_3C_2 phase. The oxygen (12.75 at%) and fluorine (2.52 at%) content, marked in red and light blue, respectively, indicate the formation of –O and –F surface terminations during the etching process. These functional groups enhance hydrophilicity, provide active sites for electrochemical reactions, and improve charge transfer properties, which are critical for applications such as hydrogen evolution reactions (HER) and energy storage [46]. The surface chemistry, shaped by the presence of these terminations, makes $Ti_3C_2T_x$ MXene a highly promising candidate for use in electrochemical systems, including supercapacitors and water electrolysers, due to its unique combination of electrical conductivity, chemical stability, and surface reactivity.

X-ray photoelectron spectroscopy (XPS) was utilized to determine the surface chemical composition and bonding states of the synthesized MXene. The survey scan (Fig. 3a) confirmes the presence of Titanium (Ti), Carbon (C), Oxygen (O), Fluorine (F), and trace Chlorine (Cl). Analysis of the high-resolution C 1s spectrum (Fig. 3c) revealed a distinct peak component around 282 eV, characteristic of Ti–C bonds within the MXene lattice, alongside peaks for adventitious carbon and carbon-oxygen bonds. The Ti 2p spectrum (Fig. 3b) exhibited broad features consistent with multiple Ti chemical states, including Ti–C, Ti–O, and Ti–F bonds typical for functionalized MXene. Strong signals in the F 1s (centered ∼685–686 eV, Fig. 3d) and O 1s (broad peak ∼530–532 eV, Fig. 3e) spectra confirm the presence of significant –F, –O, and –OH surface terminations, which are expected outcomes of the LiF/HCl etching procedure. These results collectively verify the successful synthesis and surface functionalization of the Ti-based MXene [47]. In Fig. 3f, X-ray diffraction (XRD) pattern of the MAX phase (blue) shows a distinct (002) peak at 9.56° (2θ), corresponding to a d-spacing of 9.3 Å, calculated using Bragg's law [48] with a Cu Kα wavelength of 1.54056Å. This peak reflects the interlayer spacing between Ti_3C_2 layers in the hexagonal crystal structure (P63/mmc) [49]. Additional peaks at 18.8° (004), 39.1° (104), 41.6° (105), 48.5° (107), and minor peaks at 60.6° (2-1-0) and 78.5°C (2-1-8) confirm the presence of characteristic planes, indicating a well-crystallized MAX phase. The absence of extraneous peaks suggests high phase purity, with no significant impurities detected. For the XRD analysis of the MXene (red), the (002) peak observed at 6.1° (2θ) corresponds to a d-spacing of 14.48Å, which is significantly larger than the original MAX phase (002) peak. This increase in interlayer spacing is expected after etching the Al layer [50], as it allows the layers to delaminate, creating a single-layer MXene. The larger d-spacing reflects the successful exfoliation of the MXene layers. The minor peaks at 18.5° (004) and 19.5° (006) suggest the multilayer nature of some residual MXene layers. The thickness of a single MXene layer is around 1–2 nm, which is consistent with typical MXene morphology [51]. The aforementioned characterizations can prove that the successful synthesis of single-layer MXene.

Electrochemical measurements were performed under iR-corrected conditions to evaluate the HER activity of the synthesized electrodes (Fig. 4a). The polarization curves clearly demonstrate that the incorporation of GO and CB into the MXene framework significantly enhances catalytic performance. The MXene–GO–CB composite exhibited the lowest

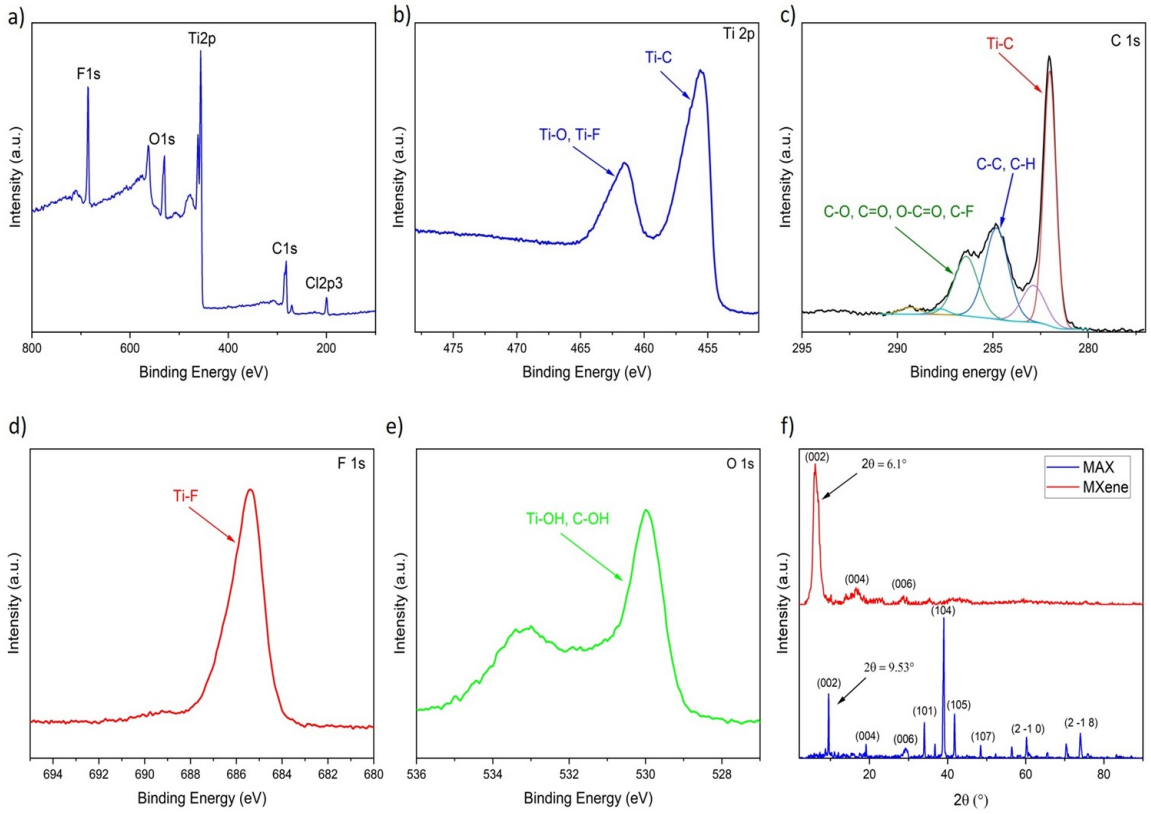

FIG. 3. XPS and XRD characterization of $Ti_3C_2T_x$ MXene synthesized from Ti_3AlC_2 MAX phase. (a) The full XPS survey spectrum. (b) The high-resolution Ti 2p spectrum. (c) The C 1s spectrum. (d) The F 1s peak. (e) The O 1s spectrum. (f) XRD patterns of the MAX phase (blue) and exfoliated MXene (red)

overpotential of 196 mV at 10 mA cm^{-2}, outperforming pristine MXene (300 mV), MXene–GO (248 mV), and MXene–CB (266 mV). This pronounced improvement highlights the synergistic effect of GO and CB in facilitating charge transfer, improving conductivity, and providing additional active sites, thereby accelerating HER kinetics compared to single-component or binary composites. The Tafel slope, which offers insight into the reaction mechanism, was determined by plotting overpotential against the logarithm of current density following the equation [52]:

$$b = \frac{\Delta\eta}{\Delta(\log j)}$$

where b is the Tafel slope, typically expressed in mV/dec Higher Tafel slope values often indicate a one-electron transfer rate-limiting step, while lower values suggest faster kinetics or differing rate determining steps [53].

The catalytic kinetics of the prepared electrodes were further evaluated by Tafel slope analysis (Fig. 4b). Pristine MXene exhibited a Tafel slope of 113.57 mV dec^{-1}, while the binary composites MXene–GO and MXene–CB showed slopes of 113.95 mV dec^{-1} and 152.8 mV dec^{-1}, respectively. In contrast, the MXene–GO–CB composite achieved the lowest Tafel slope of 96.35 mV dec^{-1}, confirming its faster HER kinetics. These results indicate that the synergistic combination of GO and CB with MXene not only lowers the overpotential but also accelerates the reaction pathway, facilitating more efficient electron transfer and hydrogen evolution compared to individual or binary systems. The observations can be attributed to electron density distribution and interfacial interactions, where MXene's metallic conductivity ensures rapid charge mobility, while GO and CB enhance the exposure of active sites. MXene's surface functional groups (-OH, -F, -O) contribute to its catalytic behavior, influencing intermediate adsorption and reaction pathways. The presence of GO and CB in MXene-GO-CB/NF enhances the catalytic activity by increasing active surface area and promoting mass transport, making it a favorable electrode for reducing overpotential.

The long-term durability of the MXene–GO–CB/NF composite electrocatalyst was evaluated by chronopotentiometry and LSV measurements (Fig. 5). Under a constant current density of 100 mA cm^{-2}, the electrode exhibited rapid stabilization within the first few minutes, followed by a steady operation over 50 h with only a slight potential increase of $\sim$0.07 V, confirming its excellent structural and electrochemical robustness. Furthermore, the LSV curves recorded before and after the stability test showed a minor performance decay, with the overpotential at 10 mA cm^{-2} shifting from 196 to 230 mV. This negligible change (34 mV) highlights the strong durability of the MXene–GO–CB/NF electrode under harsh and continuous HER operating conditions, underscoring its potential for practical water electrolysis applications.

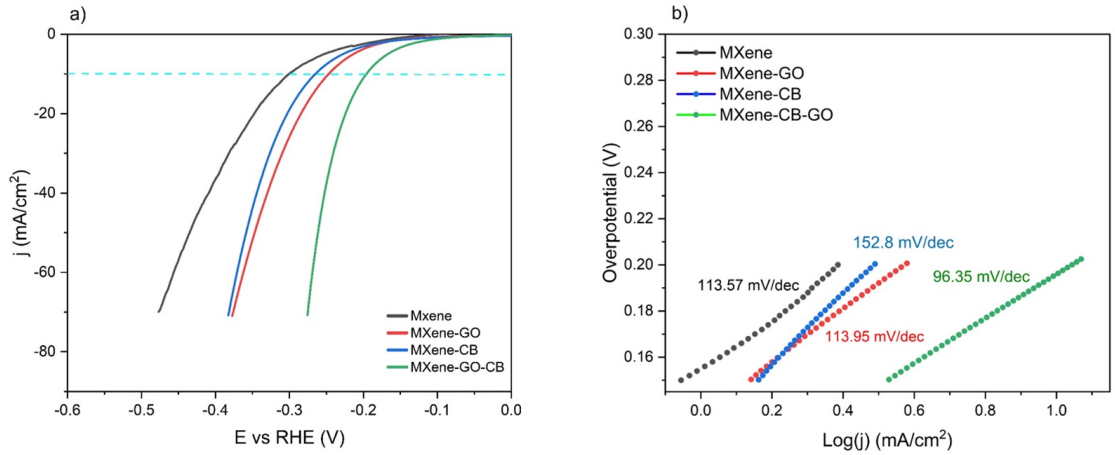

FIG. 4. Electrochemical performance of MXene, MXene-GO, MXene-CB, and MXene-GO-CB composite electrodes in 1 M KOH. (a) Half-cell polarization curves of all electrodes. (b) Corresponding Tafel plots

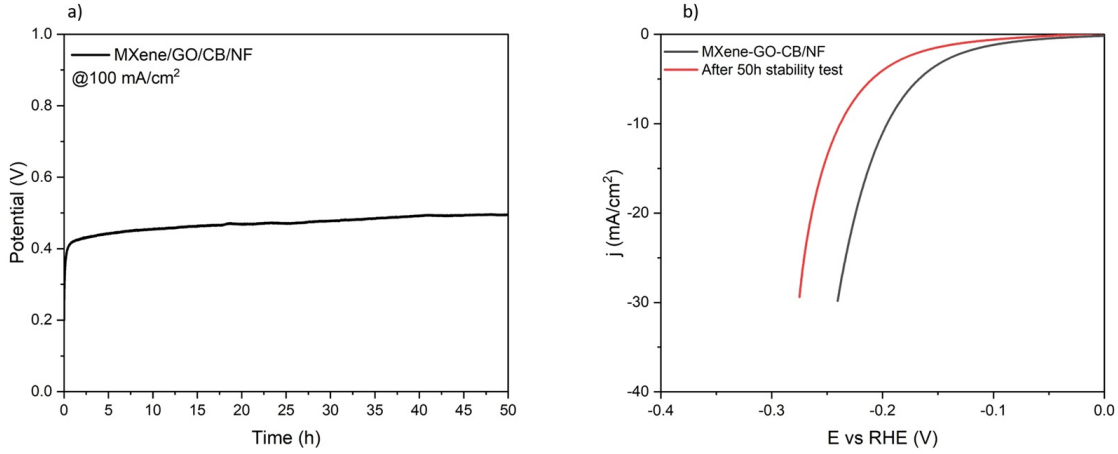

FIG. 5. Stability evaluation of the MXene-GO-CB/NF composite electrocatalyst. (a) Chronopotentiometry measurement at a constant current density of 100 mA cm^{-2} for 50 h. (b) LSV polarization curves recorded before and after the 50 h stability test

Electrochemical impedance spectroscopy (EIS) measurements were conducted at fixed potentials of 1.6 V vs. RHE for OER and −0.3 V vs. RHE for HER. The measurements frequency range is from 0.1 Hz to 100 kHz with a small AC amplitude of 5 mV. The Nyquist plots for both OER and HER were present in Fig. 6, with the real part of the impedance (Z') on the x-axis and the imaginary part (Z'') on the y-axis. The Nyquist plot analysis shows that the MXene/NF electrode exhibits distinct charge transfer resistance (R_{ct}) values for the OER and HER processes, with R_{ct} measured at 1.02 Ω for OER and 0.6 Ω for HER. The relatively low R_{ct} for HER, in particular, indicates more efficient electron transfer, suggesting higher conductivity and catalytic performance under alkaline conditions. These results underscore the MXene/NF electrode's effectiveness as a bifunctional catalyst, capable of facilitating both oxygen and hydrogen evolution reactions with promising efficiency, making it a viable candidate for applications in sustainable hydrogen production and alkaline water electrolysis.

The double-layer capacitance, C_{dl}, is a parameter that represents the capacitance of the electrical double layer formed at the interface between the electrode surface and the electrolyte solution. When a potential is applied to the electrode, ions from the electrolyte are attracted to the surface, creating a double layer of charges with a capacitance that depends on the surface area of the electrode.

Fig. 7a presents cyclic voltammetry (CV) curves for the MXene/Nickel Foam (NF) electrode recorded at various scan rates (1, 2, 3, 4, and 5 mV/s). These curves illustrate the capacitive behavior of the electrode in the non-faradaic region which is from −140 mV to −35 mV, confirming the formation of an electrochemical double layer. The gradual increase in current density with increasing scan rate indicates enhanced charge storage capabilities and surface area exposure. Chosen anodic and cathodic currents were shown in Fig. 7b. To calculate C_{dl}, the linear fitting of $\Delta j/2$ versus scan rate is plotted in Fig. 7c, revealing a double layer capacitance per unit area value of 73.6 mF/cm^2.

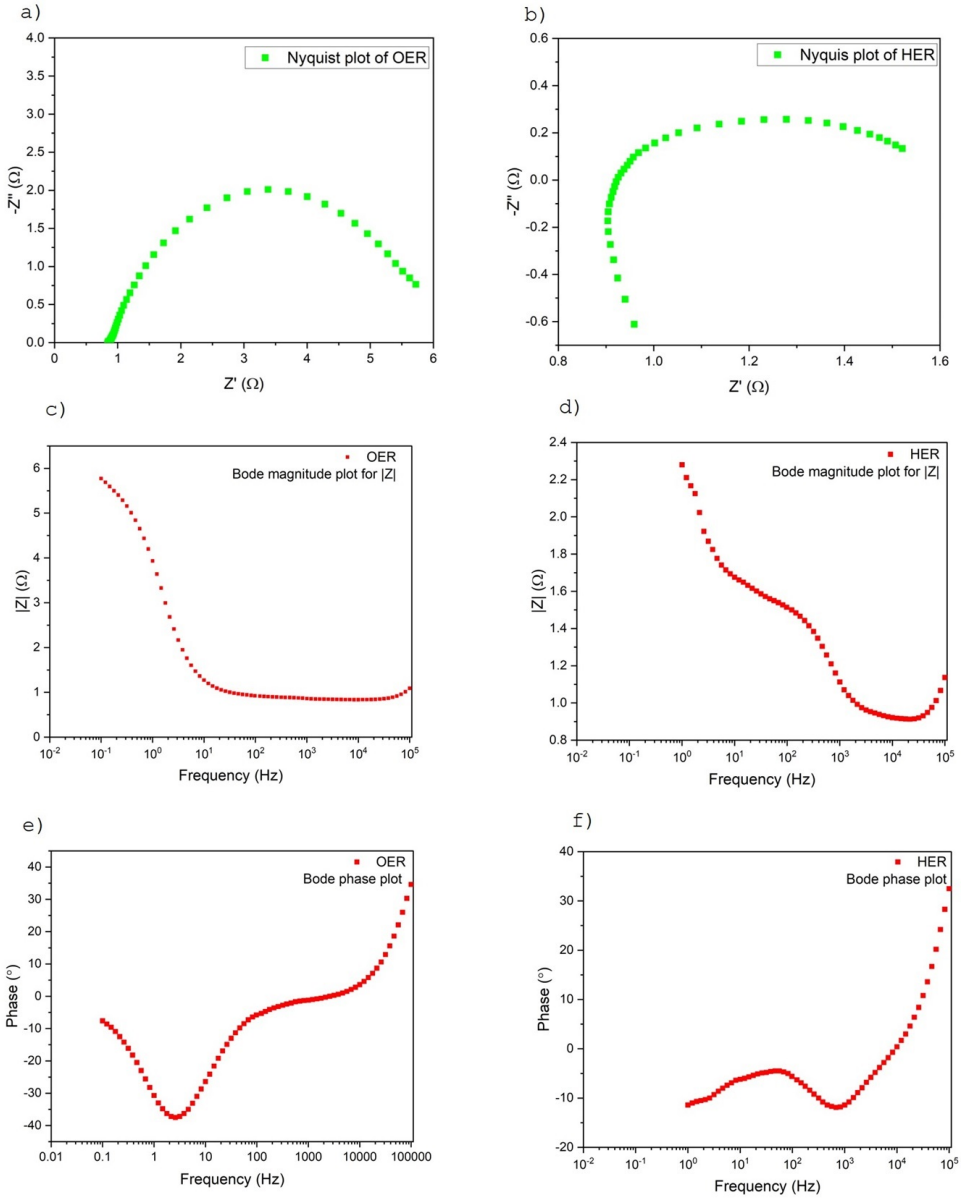

FIG. 6. Electrochemical Impedance Spectroscopy (EIS) analysis of the electrode during the Oxygen Evolution Reaction (OER) and Hydrogen Evolution Reaction (HER). (a, b) Nyquist plots for OER and HER, respectively, showing the real (Z') and imaginary ($-Z''$) components of impedance. (c, d) Bode magnitude plots showing $|Z|$ as a function of frequency for OER and HER, respectively. (e, f) Bode phase plots displaying the phase angle versus frequency for OER and HER, respectively

The specific capacitance, C_s, represents the intrinsic capacitance per unit area of a material in a given electrolyte, and it can vary based on the electrode material and electrolyte conditions. The specific capacitance values (C_s) for a flat standard with 1 cm^2 of the real surface area that is generally in the range of 20 to 60 μF cm^{-2} (40 μF cm^{-2} was taken as the average value) [54]. For our electrode with 1.6 cm^2 surface area, Cs is 64 μFcm^{-2}. These results indicate that the MXene/NF composite provides substantially higher specific capacitance than nickel foam alone, likely due to large electrochemical surface area and elevated capacitance of MXene.

ESCA was calculated by using C_{dl} and C_s [55] using the following equation:

$$\text{ECSA} = \frac{C_{dl}}{C_s}$$

The electrochemical surface area (ECSA) of the MXene/NF composite shows 1840 cm^2. These values are notably higher than those typically observed for conventional electrode materials like pristine nickel foam, which commonly exhibit lower ECSAs due to their relatively limited surface areas and active sites. The enhanced ECSA values observed in the MXene/NF composite are indicative of the substantial increase in active surface area provided by MXenes, which likely contributes to its superior electrocatalytic performance in both OER and HER processes.

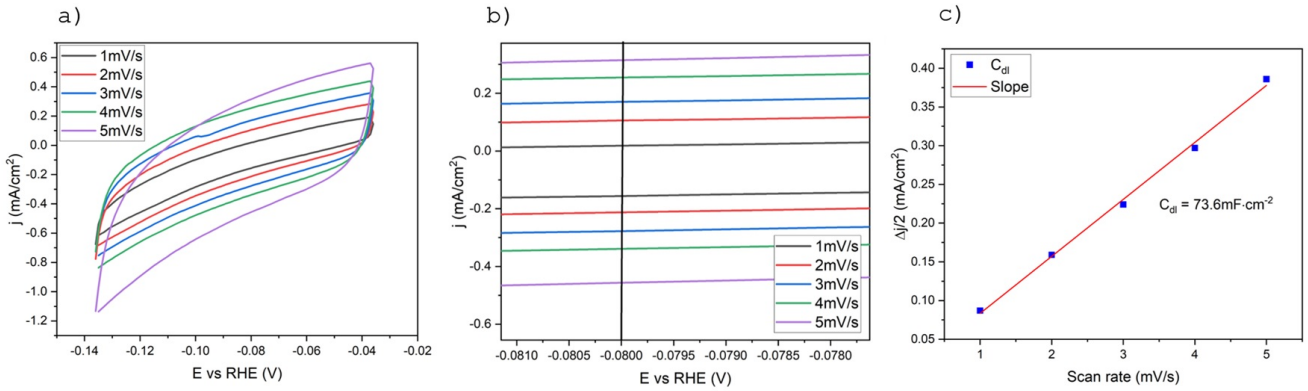

FIG. 7. (a) Cyclic voltammetry curves at various scan rates (1–5 mV s^{-1}) for C_{dl} determination, (b) current density differences (Δj) versus potential at a fixed potential, and (c) linear fitting of Δj/2 versus scan rate for C_{dl} extraction

4. Conclusion

In this study, we successfully synthesized $Ti_3C_2T_x$ MXene and its composite electrodes with graphene oxide (GO) and carbon black (CB) on nickel foam (NF) substrates for efficient water splitting applications. Structural and compositional analyses, including SEM, XRD, and XPS, confirmed the successful etching of the MAX phase, formation of single-layer $Ti_3C_2T_x$ MXene sheets, and the presence of functional surface terminations beneficial for catalytic activity. The incorporation of GO and CB into the MXene framework significantly enhanced electrochemical performance by improving conductivity, stability, and active surface area.

Electrochemical evaluations demonstrated that the MXene–GO–CB composite electrode exhibited a remarkably low overpotential of 196 mV at 10 mA cm^{-2} for the hydrogen evolution reaction (HER), outperforming pristine MXene and binary composites. The reduced Tafel slope (96.35 mV dec^{-1}), low charge-transfer resistance (R_{ct}), and high electrochemical surface area (ECSA = 1840 cm^2) confirmed improved reaction kinetics and abundant active sites. Moreover, the electrode maintained good long-term stability, with only minimal performance degradation after 50 h of continuous operation at 100 mA cm^{-2}, highlighting its robustness under harsh alkaline conditions.

Overall, the synergistic effects of MXene, GO, and CB on NF resulted in a highly efficient, durable, and cost-effective electrocatalyst for hydrogen production. This work provides a promising strategy for the rational design of advanced MXene-based composites for large-scale and sustainable water electrolysis applications. Future studies should focus on optimizing composite architectures, scaling up synthesis techniques, and integrating these materials into practical electrolyzer systems for renewable hydrogen generation.

References

[1] Sampene A.K., Li C., Wiredu J. An outlook at the switch to renewable energy in emerging economies: The beneficial effect of technological innovation and green finance. *Energy Policy*, 2024, **187**, P. 114025.
[2] Ehteshami, S.M.M., Chan S.H. The role of hydrogen and fuel cells to store renewable energy in the future energy network – potentials and challenges. *Energy Policy*, 2014, **73**, P. 103–109.
[3] Anderson D., Leach M. Harvesting and redistributing renewable energy: on the role of gas and electricity grids to overcome intermittency through the generation and storage of hydrogen. *Energy Policy*, 2003, **32**(14), P. 1603–1614.
[4] Luo Z., Hu Y., Xu H., Gao D., Li W. Cost-Economic analysis of hydrogen for China's fuel cell transportation field. *Energies*, 2020, **13**(24), P. 6522.
[5] Olivier P., Bourasseau C., Bouamama Pr.B. Low-temperature electrolysis system modelling: A review. *Renewable and Sustainable Energy Reviews*, 2017, **78**, P. 280–300.
[6] Karthikeyan S.C., Sidra S., Ramakrishnan S., Kim D.H., Sagayaraj P.J., Sekar K., Yoo D.J. Heterostructured NiO/IrO_2 synergistic pair as durable trifunctional electrocatalysts towards water splitting and rechargeable zinc-air batteries: An experimental and theoretical study. *Applied Catalysis B Environment and Energy* 2024, **355**, P. 124196.
[7] Qadeer M.A., Zhang X., Farid M.A., Tanveer M., Yan Y., Du S., Huang Z., Tahir M., Zou J. A review on fundamentals for designing hydrogen evolution electrocatalyst. *Journal of Power Sources*, 2024, **613**, P. 234856.
[8] Tang J., Xu X., Tang T., Zhong Y., Shao Z. Perovskite-Based electrocatalysts for Cost-Effective Ultrahigh-Current-Density water splitting in anion exchange membrane electrolyzer cell. *Small Methods*, 2022, **6**(11).
[9] Amani A.M., Tayebi L., Vafa E., Jahanbin A., Abbasi M., Vaez A., Kamyab H., Chelliapan S. Innovation applications of MXenes in biomedicine. *Materials Today Communications*, 2024, **40**, P. 109929.
[10] Naguib M., Kurtoglu M., Presser V., Lu J., Niu J., Heon M., Hultman L., Gogotsi Y., Barsoum M.W. *Two-Dimensional Nanocrystals Produced by Exfoliation of Ti_3AlC_2*, 2023.
[11] Fu L., Xia W. MAX phases as nanolaminate materials: chemical composition, microstructure, synthesis, properties, and applications. *Advanced Engineering Materials*, 2020, **23**(4).
[12] Haemers J., Gusmão R., Sofer Z. Synthesis protocols of the most common layered carbide and nitride MAX phases. *Small Methods*, 2020, **4**(3).
[13] Sokol M., Natu V., Kota S., Barsoum M.W. On the Chemical Diversity of the MAX Phases. *Trends in Chemistry*, 2019, **1**(2), P. 210–223.
[14] Barsoum M.W., Radovic M. Elastic and mechanical properties of the MAX phases. *Annual Review of Materials Research* 2011, **41**(1), P. 195–227.

[15] Wei Y., Zhang P., Soomro R. A., Zhu Q., Xu B. Advances in the synthesis of 2D MXenes. *Advanced Materials*, 2021, **33**(39).

[16] Kajiyama S., Szabova L., Iinuma H., Sugahara A., Gotoh K., Sodeyama K., Tateyama Y., Okubo M., Yamada A. Enhanced Li-Ion accessibility in MXENE titanium carbide by steric chloride termination. *Advanced Energy Materials*, 2017, **7**(9).

[17] Naguib M., Kurtoglu M., Presser V., Lu J., Niu J., Heon M., Hultman L., Gogotsi Y., Barsoum M.W. Two-Dimensional nanocrystals produced by exfoliation of TI_3ALC_2. *Advanced Materials*, 2011, **23**(37), P. 4248–4253.

[18] Yang S., Zhang P., Wang F., Ricciardulli A.G., Lohe M.R., Blom P.W.M., Feng X. Fluoride-Free synthesis of Two-Dimensional titanium carbide (MXENE) using a binary aqueous system. *Angewandte Chemie International Edition*, 2018, **57**(47), P. 15491–15495.

[19] Ni Q.-Y., He X.-F., Zhou J.-L., Yang Y.-Q., Zeng Z.-F., Mao P.-F., Luo Y.-H., Xu J.-M., Jiang B., Wu Q., Wang B., Qin Y.-Q., Gong L.-X., Tang L.-C., Li S.-N. Mechanical tough and stretchable quaternized cellulose nanofibrils/MXene conductive hydrogel for flexible strain sensor with multi-scale monitoring. *Journal of Material Science and Technology*, 2024, **191**, P. 181–191.

[20] Jiang M., Wang D., Kim Y., Duan C., Talapin D.V., Zhou C. Evolution of Surface Chemistry in Two-Dimensional MXEnES: From mixed to Tunable Uniform Terminations. *Angewandte Chemie*, 2024, **136**(37).

[21] Cao, Fangcheng, et al. Recent Advances in Oxidation Stable Chemistry of 2D MXenes. *Advanced Materials*, 2022, **34**(13), P. 2107554.

[22] Soomro, Razium A., et al. Progression in the Oxidation Stability of MXenes. *Nano-Micro Letters*, 2023, **15**(1), P. 18.

[23] Iqbal, Aamir, et al. Improving Oxidation Stability of 2D MXenes: Synthesis, Storage Media, and Conditions. *Nano Convergence*, 2021, **8**(1), P. 16.

[24] Gao X., Du X., Mathis T.S., et al. Maximizing ion accessibility in MXene-knotted carbon nanotube composite electrodes for high-rate electrochemical energy storage. *Nat Commun*, 2020, **11**, P. 6160.

[25] Meng, Weisong, et al. Alkalized MXene/Carbon Nanotube Composite for Stable Na Metal Anodes. *RSC Advances*, 2024, **14**(17), P. 12030–12037.

[26] Iravani, Siavash, et al. Advancements in MXenes and Mechanochemistry: Exploring New Horizons and Future Applications. *Materials Advances*, 2024, **5**(21), P. 8404–8418.

[27] He Lei, et al. Advances and Challenges in MXene-Based Electrocatalysts: Unlocking the Potential for Sustainable Energy Conversion. *Materials Horizons*, 2024, **11**(18), P. 4239–4255.

[28] Zhang, Qingxiao, et al. Synthesis and Design Strategies of MXene Used as Catalysts. *ChemCatChem*, 2024, **16**(22).

[29] Zhou Tianzhu, et al. Super-Tough MXene-Functionalized Graphene Sheets. *Nature Communications*, 2020, **11**(1), P. 2077.

[30] Li Xiao-Peng, et al. Reshapable MXene/Graphene Oxide/Polyaniline Plastic Hybrids with Patternable Surfaces for Highly Efficient Solar-Driven Water Purification. *Advanced Functional Materials*, 2021, **32**(15).

[31] Gong Kaili, et al. MXene as Emerging Nanofillers for High-Performance Polymer Composites: A Review. *Composites Part B: Engineering*, 2021, **217**, P. 108867.

[32] Iravani Siavash, et al. Synergistic Advancements: Exploring MXene/Graphene Oxide and MXene/Reduced Graphene Oxide Composites for Next-Generation Applications. *FlatChem*, 2024, **48**, P. 100759.

[33] Liu Qi, et al. Improved Anti-Corrosion Behaviour of an Inorganic Passive Film on Hot-Dip Galvanised Steel by Modified Graphene Oxide Incorporation. *Corrosion Science*, 2020, **174**, P. 108846.

[34] Yin Yiming, et al. Distinct Ion Transport Behavior between Graphene Oxide and UV-Irradiated Reduced Graphene Oxide Membranes. *Chemical Engineering Journal*, 2024, **493**, Aug., P. 152304.

[35] Amir Reza Salasel, et al. Role of Graphene Concentration on Electrochemical and Tribological Properties of Graphene-Poly(Methyl Methacrylate) Composite Coatings. *Journal of Composite Materials*, 2023, **57**(24), P. 3877–3896.

[36] Su, Liwei, et al. N-Doped Carbon Nanolayer Modified Nickel Foam: A Novel Substrate for Supercapacitors. *Applied Surface Science*, 2020, **546**, P. 148754–148754.

[37] Zhang Jiaoyuan, et al. Construction of ZnO@Co3O4-Loaded Nickel Foam with Abrasion Resistance and Chemical Stability for Oil/Water Separation. *Surface and Coatings Technology*, 2019, **357**, P. 244–251.

[38] Das, Manisha, et al. Three-Dimensional Nickel and Copper-Based Foam-In-Foam Architecture as an Electrode for Efficient Water Electrolysis. *Catalysis Today*, 2023, **424**(1), P. 113836.

[39] Ao Guang-Hong, et al. Construction of Hierarchical Porous Architecture on Ni Foam for Efficient Oxygen Evolution Reaction Electrode. *Frontiers in Materials*, 2021, **8**.

[40] Yu K., Zhang J., Hu Y., Wang L., Zhang X., Zhao B. Ni Doped Co-MOF-74 Synergized with 2D Ti3C2Tx MXene as an Efficient Electrocatalyst for Overall Water-Splitting. *Catalysts*, 2024, **14**(3), P. 184.

[41] Shi X., Yu Z., Liu Z., Cao N., Zhu L., Liu Y., Zhao K., Shi T., Yin L., Fan Z. Scalable, High-Yield Monolayer MXene Preparation from Multilayer MXene for Many Applications. *Angewandte Chemie*, 2024.

[42] Jiang S., Lu L., Song Y. Recent Advances of Flexible MXene and its Composites for Supercapacitors. *Chemistry – a European Journal* 2024, **30**(24).

[43] Khanal R., Irle S. Effect of surface functional groups on MXene conductivity. *The Journal of Chemical Physics*. 2023, **158**(19).

[44] Zhang Wei, et al. Effect of Carbon Black Concentration on Electrical Conductivity of Epoxy Resin–Carbon Black–Silica Nanocomposites. *Journal of Materials Science*, 2007, **42**(18), P. 7861–7865.

[45] Abdullah N., Ishak N.A.I.M., Tan K.H., Zaed M.A., Saidur R., Pandey A.K. Investigating the impact of various etching agents on Ti_3C_2Tx MXene synthesis for electrochemical energy conversion. *FlatChem*, 2024, **47**, P. 100730.

[46] Verger L., Xu C., Natu V., Cheng H.-M., Ren W., Barsoum M.W. Overview of the synthesis of MXenes and other ultrathin 2D transition metal carbides and nitrides. *Current Opinion in Solid State and Materials Science*, 2019, **23**(3), P. 149–163.

[47] Miao B., Bashir T., Zhang H., Ali T., Raza S., He D., Liu Y., Bai J. Impact of various 2D MXene surface terminating groups in energy conversion. *Renewable and Sustainable Energy Reviews*, 2024, **199**, P. 114506.

[48] Singh, Iqbal, et al. Modification of the Properties of Titanium Carbide MXene by Ag Doping via Ion Implantation for Quantum Dot-Sensitized Solar Cell Applications. *Journal of Electronic Materials*, 2024, **53**(9), P. 5007–5017.

[49] González A. 1.5 X-Ray Crystallography: Data Collection Strategies and Resources. *Comprehensive Biophysics*, 2012, P. 64–91.

[50] Mamanazirov J.I., Ruzimuradov O.N., Mamatkulov Sh.I. THE IMPACT OF 2D MXENE ON ALUMINA BASED INKS FOR DIRECT INK WRITING. *Ceramics International*, 2025, **51**(12PA), P. 15725–15732.

[51] Yun T., Kim H., Iqbal A., Cho Y.S., Lee G.S., Kim M., Kim S.J., Kim D., Gogotsi Y., Kim S.O., Koo C.M. Electromagnetic shielding of monolayer MXENE assemblies. *Advanced Materials*, 2020, **32**(9).

[52] Murthy A.P., Theerthagiri J., Madhavan J. Insights on Tafel constant in the analysis of hydrogen evolution reaction. *The Journal of Physical Chemistry C* 2018, **122**(42), P. 23943–23949.

[53] Thomas J.G.N. Kinetics of electrolytic hydrogen evolution and the adsorption of hydrogen by metals. *Transactions of the Faraday Society*, 1961, **57**, P. 1603.

[54] Sergiienko S.A., Lajaunie L., Rodríguez-Castellón E., et al. Composite MAX phase/MXene/Ni electrodes with a porous 3D structure for hydrogen evolution and energy storage application. *RSC Advances*, 2024, **14**(5), P. 3052–3069.
[55] Granozzi G., Alonso-Vante N. *Electrochemical Surface Science: Basics and applications*, MDPI, 2019.

Submitted 29 July 2025; revised 27 September 2025; accepted 4 December 2025

Information about the authors:

Javlonbek Mamanazirov – Institute of Materials Science, Uzbekistan Academy of Sciences, Chingiz Aytmatov 2B St., Tashkent, 100084, Uzbekistan; National Research Institute of Renewable Energy Sources, Ministry of Energy, Bodomzor Yuli 2B St., Tashkent, 100084, Uzbekistan; ORCID 0009-0004-2222-2461; j.mamanazirov@imssolar.uz

Shavkat Mamatkulov – Institute of Materials Science, Uzbekistan Academy of Sciences, Chingiz Aytmatov 2B St., Tashkent, 100084, Uzbekistan; Institute of Fundamental and Applied Research under TIIAME National Research University, Mirzo Ulug'bek district, Qori Niyaziy street 39, Tashkent, 100000, Uzbekistan; ORCID 0000-0002-9694-4430; mi-shavkat@yandex.ru

Maxfuza Jumayeva – Institute of Materials Science, Uzbekistan Academy of Sciences, Chingiz Aytmatov 2B St., Tashkent, 100084, Uzbekistan; m.jumayeva1988@gmail.com

Khakimjan Butanov – Institute of Materials Science, Uzbekistan Academy of Sciences, Chingiz Aytmatov 2B St., Tashkent, 100084, Uzbekistan; ORCID 0000-0003-1805-9089; kh.butanov@gmail.com

Wen He – School of Materials Science and Engineering, Anhui University, Hefei, 230601, China; ORCID 0000-0002-7673-7274; hewen@ahu.edu.cn

Jingxiang Low – School of Physical Science and Technology, Tiangong University, Tianjin, 300387, P.R. China; ORCID 0000-0002-2486-6357; jxlow@ustc.edu.cn

Odilhuja Parpiev – Institute of Materials Science, Uzbekistan Academy of Sciences, Chingiz Aytmatov 2B St., Tashkent, 100084, Uzbekistan; ORCID 0000-0002-7494-3445; o.parpiev@imssolar.uz

Olim Ruzimuradov – Turin Polytechnic University in Tashkent, Tashkent, 100095, Uzbekistan; ORCID 0000-0002-9186-9080; o.ruzimuradov@new.polito.uz

Conflict of interest: the authors declare no conflict of interest.